Vol.65: e22210316, 2022
https://doi.org/10.1590/1678-4324-2022210316
ISSN 1678-4324 Online Edition

Article - Engineering, Technology and Techniques

An Early Prediction of Tumor in Heart by Cardiac Masses Classification in Echocardiogram Images Using Robust Back Propagation Neural Network Classifier

Manikandan Annamalai[1*]
https://orcid.org/0000-0001-7567-2379

Ponni Bala Muthiah[2]
https://orcid.org/0000-0001-9802-1421

[1]Vivekanandha College of Technology for Women, Department of ECE , Tiruchengode,Tamil Nadu, India; [2]Velalar College of Engineering and Technology, Department of Biomedical Engineering, Erode, Tamil Nadu, India.

Editor-in-Chief: Alexandre Rasi Aoki
Associate Editor: Raja Soosaimarian Peter Raj

Received: 17-May-2021; Accepted: 30-Sep-2021.

*Correspondence: mani85a@gmail.com; Tel.: +91-9976311940 (M.A.).

HIGHLIGHTS

- Cardiac mass image noise is diminished by Adaptive Vector Median Filter.
- The masses were automatically segmented dependent on Linear Iterative Vessel Segmentation strategy followed by texture features extracted utilizing the Multiscale Local Binary Pattern method.
- The classification done by Robust back propagation neural network.

ABSTRACT: Identification and classification of intracardiac masses in echocardiogram is one of the significant processes in the diagnosis of cardiovascular disease. A robust back propagation neural network (RBPNN) technique is used to conquer every single conventional-issue utilizing the echocardiogram image analysis for this work, which consists of four phases such as noise removal, automatic segmentation, feature extraction, and intracardiac masses classification. Initially, the noise is diminished from the echocardiogram images utilizing the adaptive vector median filter (AVMF). Then, linear iterative vessel segmentation (LIVS) is applied for automatic segmentation of the masses followed by the extraction of texture features using the multiscale local binary pattern (MS-LBP) approach. Finally, RBPNN is employed to classify the heart mass from the images of echocardiogram with the layered kernel for the system combination. Extensive simulation results obtained using proposed AVMF-MS-LBP based RBPNN approach disclosed the superiority over existing intracardiac mass detection and classification approaches in terms of accuracy of 98.85%.

Keywords: Echocardiogram; Cardiac Masses; Linear Iterative Vessel Segmentation; Multiscale Local Binary Pattern; Robust Back Propagation Neural Network.

INTRODUCTION

Intracardiac masses are irregular structures discovered inside or close by the heart. These structures lead to genuine cardiovascular issues and require good findings for brief resection and treatment [1]. There are two essential kinds of intra heart masses to be explicit: tumor and thrombi. The cancer is the growth of a bit of body realized by the unpredictable improvement of tissues, which shows compactness and thrombi is a blood clot (solid mass of platelets) [2]. The Echocardiogram intracardiac tumor (Figure 1(a)) and thrombi (Figure 1(b)) is shown in Figure 1.

Therefore, the requirement for a computerized recognition is expanding, which can improve analytic precision and guide in which a specialist should be recommended [3]. Because the relative echocardiogram inception of the two masses and the picture quality are hazardous, including the vast measure of speckle noise [4], the sign forgetting about the rarities [5] and missing shapes [6].

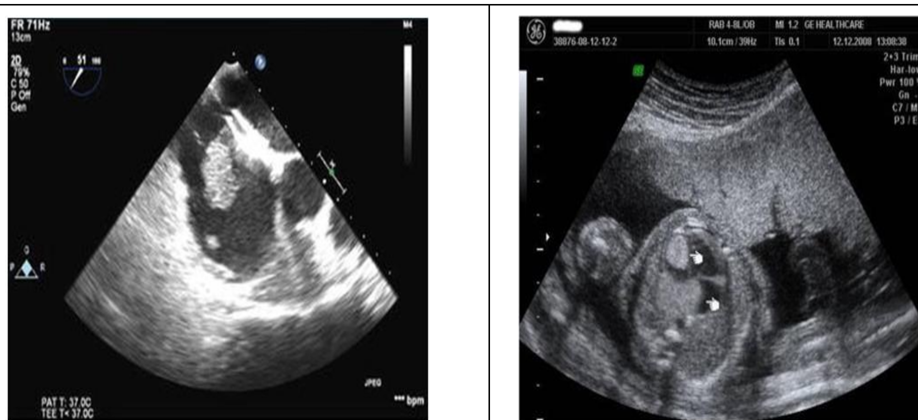

a) Intracardiac Tumor | b) Intracardiac Thrombi

Figure1. (a) Intracardiac tumor and (b) Intracardiac thrombi

Research Background

Assessment of ultrasound images has been utilized effectively in the computer-aided design of cardiovascular infection, to distinguish the proof of necessary ultrasound emphasis in the early forecast of stroke [7], in the construction of an aid system with the selection based on fuzzy rules for the prognosis of the coronary arteries disease [8], and in the use of adaptive blocking adaptive methodologies in the dynamics of the wall and the plate of the carotid artery [9]. The neuronal culture was recommended to identify and phase out echocardiograms of intracardiac tumors by the hundreds [10].

Usually, different types of noise removal strategies are available, such as pixel intensity correction [11], median filter based preprocessing [12], speckle-decreasing anisotropic diffusion (SRAD) found preprocessing [13] and preprocessing based on wavelet transformation strategies [14]. In [15], F-FDG uptake in cardiac tumors can differentiate benign and malignant cardiac tumors and predicts survival. In [16], recent advances in cardiovascular-relevant machine learning in the areas of image acquisition and reconstruction, image analysis, diagnostic evaluation and derivation of prognostic information are discussed. In [17], the prevalence of malignant diseases that is constantly increasing throughout the world is discussed. In [18], Kernel Collaborative Representation (KCR) is used to classify the Intra-Cardiac and Thrombi Tumors [19]. But this method failed to provide the maximum accuracy, due to improper segmentation and feature extraction. In [20], SVM-PSO method introduced for coronary tumor detection and classification.

Proposed Intracardiac Masses Detection and Classification

The proposed system consists of four phases, such as noise removal, segmentation, feature extraction, and cardiac mass classification. This technique need to manage the differentiation of pattern. Before investigating the models, the structure first needs to transfer all the images to a certain level where the examples are increasingly clear for noise-free use with AVMF, and then extract the different types of features, and the extracted features can be used to make the classification model. With this classification model framework, finally, intracardiac infection masses can be expected. Finally, the proposed framework recommends clinical treatment or guidance based on the expected intracardiac disease outcome as shown in Figure 2.

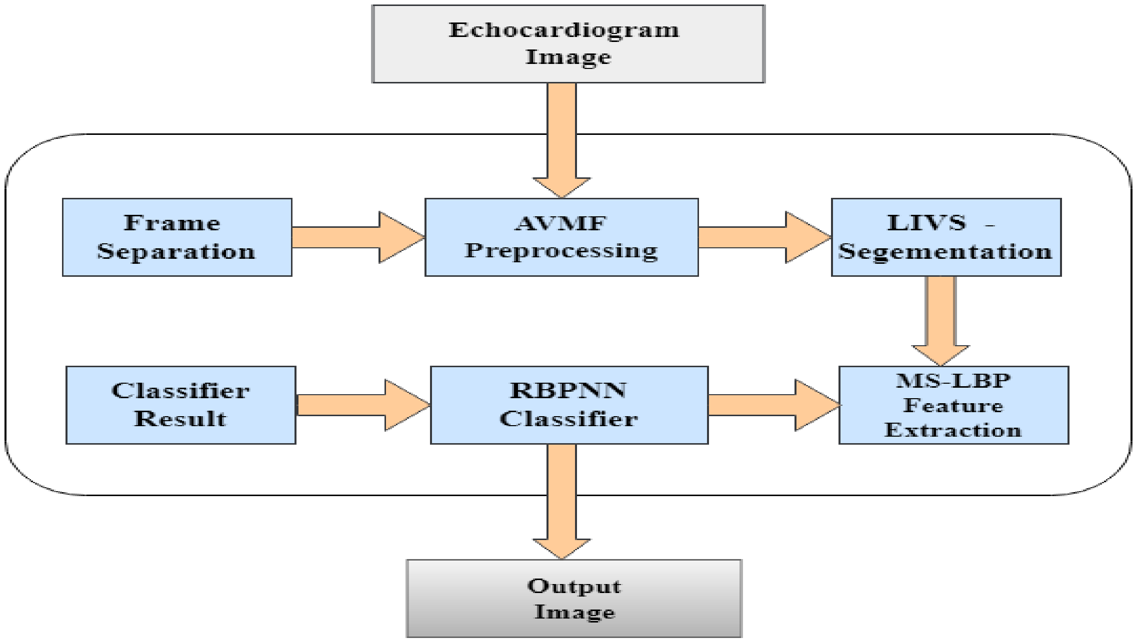

Figure 2. Proposed intracardiac Masses Detection and Classification's Block Diagram.

***Echocardiogram Image – correct only**

Adaptive Vector Median Filter

Adaptive Vector Median Filter **(**AVMF) for echocardiogram images is currently used to reduce image noise and is a type of nonlinear filtering described in the spatial domain. In this paper, adaptive VMF filter for removal of high-density speckle noise from the Echocardiogram cardiac images. A window (5 x 5) is processed over the image damaged by impulse noise. The linear non-causal prediction error will be calculated from its non-causal region of the running pixel. In the proposed filter scheme, the noisy and non-noisy pixels are categorized based on the linear non-causal prediction error. For noisy pixel, Vector Median Filter is pixel-by-pixel processing where window size is adapted based on availability of good pixels and the unobtrusive pixel is replaced with a good pixel's by vector median filter value. To remove noise from the image, the Adaptive Vector Median Filter algorithm described as in below:

Algorithm:
Input: *Scanned image from Ultrasound devices*
Output: *Preprocessed image*
Step 1: *A two-dimensional window of size 5x5 matrix is chosen and centered on the trained pixel P(a,b) in the dishonored image*.
Step 2: *Organize the pixels in the chosen window consistent with the ascending order and discover the following pixel values.*

(a) *Median pixel value indicated by* C_{med},
(b) *Maximum pixel value* (C_{max}) *and Minimum pixel value* (C_{min}) *of the organized vector V0.*

Step 3*:If the trained pixel is inside the range*
$C_{min} < P(a, b) < C_{max}$, $C_{min} > 0$ *and* $C_{max} < 255$,
processed as moral pixel and left unbothered.

Else
P (a, b) is classified as dishonored Pixel.
Step 4: *Replace the dishonored pixel P (a, b) with $C_{min.}$*
Step 5: *Step 1 to step 4 are iteratively repeated until the processing is accomplished for the entire image.*

Linear Iterative Vessel Segmentation(LIVS):

The Linear Iterative Vessel Segmentation (LIVS) strategy was mostly influenced by two factors: the feature presentation and the segmentation approach. The proposed unsupervised aggregation method requires calculating the Euclidean distance between all input data points and the Gaussian kernel for points distribution measurement $\boldsymbol{\rho_i}$of the data point$\boldsymbol{i}$. Clusters of low density and at relatively large distances of points of high density surround the centers of mass. In $\boldsymbol{\delta_i}$ the distance is measured by calculating $\boldsymbol{d_{ij}}$ the maximum distance between point 'i' and the set of points 'j' with high density. The distance $\boldsymbol{\delta_i}$ is computed utilizing Equation (1).

$$\delta_i = \begin{cases} \min_j(d_{ij}) if \rho_j > \rho_i \\ \max_j(d_{ij}) if \rho_i is the highest density \end{cases} \tag{1}$$

Where ρ_i , $\rho_j$represents the density of point i, and j and δ_i is the distance.

Global Consistency Error: Global Consistency Error (GCE) is the measure of the extent to which segmentation can be viewed as a revision of another. If the first segment is an appropriate subset of the other, then the pixel is in the filtering region and the error should be zero. If there is no subgroup relationship, then the two regions overlap in an inconsistent manner. The GCE was expressed by the following Equation (2),

$$GCE = \frac{1}{n}\min\{\sum_i(S_1, S_2, p_i) \sum_i(S_2, S_1, p_i)\} \tag{2}$$

Where segmentation error takes two segmentations S_1, S_2 as input and produces the real valued output in the range (0::1) where 0 signifies zero error.

DICE coefficient: The Dice coefficient (DICE) metrics are mostly used to validate the volume of medical image segmentation as equation (3),

$$ICE = \frac{2|A \cap B|}{|A| + |B|} \tag{3}$$

Algorithm
Input: *Preprocessed image*
Output: *Segmentation*
Step 1: *Read the image and get the representation of the input image in two color channels (Black and White).*
Step 2:*Compute the cluster centers*

(a) Register the thickness ρ and detachment measure δ by using the Equation (3) and Equation (5) individually

$$\rho_i = \sum_j exp^{-\frac{d_{ij}^2}{d_c^2}}$$

Where d_{ij} = Euclidean distance of point i and j , d_c= cutoff distance.

(b) Select the information that focuses on high thickness (ρ) and huge separation (δ) as the segmentation group.

(c) Cluster number assigned

***Step 3**: Complete the segmentation process based on the tagging results from step 2-3*

Feature Extraction: Multiscale Local Binary Pattern

When identifying an intracardiac mass in an echocardiogram sequence, cardiologists typically make a judgment based on two bases: the movement of the mass and the boundary feature or base length. Five features derived from the Multiscale Local Binary Pattern (MS-LBP) (contrast, entropy, autocorrelation, energy and homogeneity) are computed at θ =0°, 45°, 90° and 135°and d = 1. The mean density within the cluster can also classify the homogeneous and heterogeneous regions.

Mathematically the **MS-LBP** feature vector is mentioned in Equation (4) as follows.

$$V = v(s(g_o - g_c), s(g_1 - g_c) \dots \dots \dots \dots \dots \dots s(g_{p-1} - g_c)) \quad (4)$$

Where g_c is the estimation of the dimming of the average pixel and gn, (n = 0, ... P-1) demonstrates that the darkening of the neighboring pixel inside the radius R; P is the complete number of neighbors in the nearby picture adjustment. The binary feature vector is the iterative binomial factor and afterward finishes up the code that depicts the spatial structure on the neighborhood picture that has changed in the Equation (5) and (6) respectively.

$$MLBP_{P,R} = \sum_{n=0}^{P-1} S(g_n - g_c)2^n \quad (5)$$

$$s(x) = \begin{cases} 1 & x \geq 0 \\ 0 & x < 0 \end{cases} \quad (6)$$

Where s(x) = Local neighboring pixel differences, i.e.g_n-g_c = 0 (when its argument is negative otherwise one). The algorithm steps of MS-LBP are discussed in below.

Algorithm

Input: *Result of Preprocessing*

Output: *Different Types of Texture Features*

Start

Step1: *Obtain the data from preprocessing.*

Step2: *Compute the value of each binary pattern C and pick the nodes randomly from H*

If *C =* $\int_1^N Rand(H, 1, \dots, X)$

X- Nodes availability of H.

Step3: *for every Texture C_i from C*

For every random Node N_i from C_i

Compute Texture features = $\sqrt{Ni.Gm - \forall \frac{Ci.Ni.Gm}{\emptyset}}$

Step4: *Compute the result of user feedback*

Read all feature and stored to the database

Step5: *Goes to step 2 to repeat the process*

Stop

Robust Back Propagation Neural Network Classification

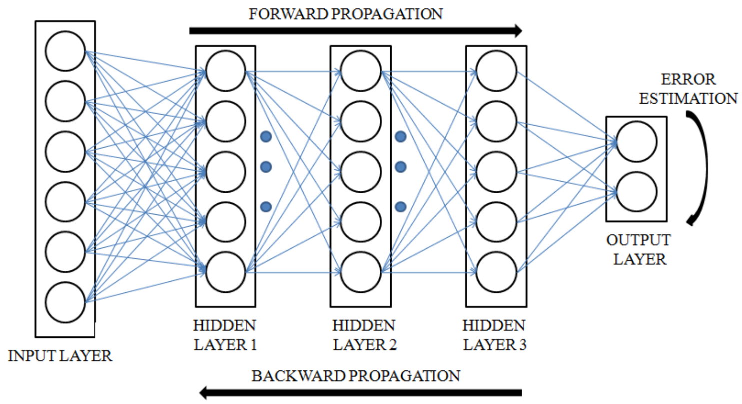

Figure 3. Robust Back Propagation Neural Network

In this section, a new learning approach based on recurring unit with a variable design to accelerate the learning period of the Robust Back Propagation Neural Network Classification (RBPNN) classifier is proposed. The behavior of a unique insect species called Weaver Ants is combined with the generic module with frequent gates to improve the execution of nervous system learning. The network is trained by a supervised learning strategy using the sigmod function. In ANN methods, for feature learning and feature classification, the information processed through the multiple levels of non-linear hierarchical layers (architectures). The architecture of Robust Back Propagation Neural Network is shown in Figure 3, it comprises of '13' input layers, '36' hidden layers and '3' output layers. The network is trained by supervised learning strategy using sigmod function, the Equation(7) is the sigmoid function.

$$\varphi_1(x) = \frac{a}{1+e^{-bx}} \tag{7}$$

Algorithm

Input: *Feature extracted values for Echocardiogram Image*

Output: *Classified intracardiac masses.*

Step 1:*Pick the quantity of neurons from input, hidden and output layers.*

Step 2: *Construct secure* ***RBPNN*** *with 3-layer Architecture.*

Step 3: *Choose the examples for training. (feature set matrix).*

Step 4: *Normalize the component vectors of each characteristic in the range of 0 & 1.*

Step 5: *Connect the neurons starting with one layer then onto the next with association loads.*

Step 6: *Initialize the pheromones (association loads) arbitrarily between - 0.5 and 0.5.*

Step 7: *Execute the training.*

Step 8: *For each Sample*

- *Calculate the output of the RBPN with current loads and store the error* (G_{min})
- *weaver ants* N_{wa} *chosen based on where* $N_{wa} < Na < NC$
- *Randomly place ants to connect neurons in the input-hidden-output layers.*
- *Calculate the output of* ***RBPNN*** *by considering the loads of neurons to be finite and storing the error value* L_{min}

Step 9: *If the output* G_{min}*> the cost of error* L_{min}*,Update pheromones only for Neurons are limited and pheromones disappear for the rest of the associations* ($G_{min} = L_{min}$)

Step 10: *Else, update the pheromones of the unlimited neuron, if the NN error is calculated,If error> 0.0001 then go to step 2, else go to step 1.*

End the process.

Experimental Images:

A total of 108real time dataset of clinical echocardiogram images were collected from the 40 patients at Department of Echocardiography, Vinayaka Mission's Kirupananda Variyar Medical College & Hospital, Salem, Tamil Nadu. A database has 108 images including 46 tumor free images,35 intracardiac thrombi and 27 were intracardiac tumors. The image format is JPEG, which are recorded using the 2D, M-mode, Color M-Mode echocardiography system equipped with a 2-4 MHz broadband phased array. The MATLAB 2018a simulator is used for training and testing the 108 real time dataset images.

Simulation Results

Input Images	Result of Preprocessing (AVMF)	Result of Segmentation (LIVS)	Type of cardiac mass
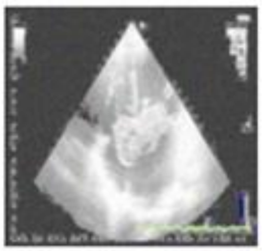 Input Image-1	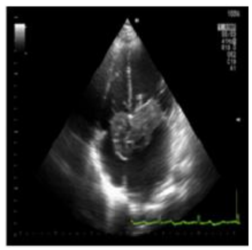	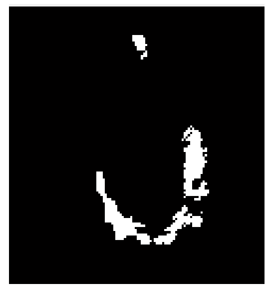	Thrombi
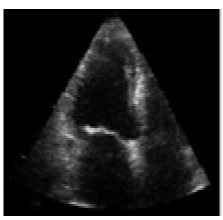 Input Image-2	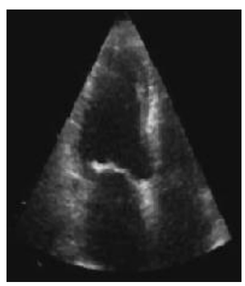	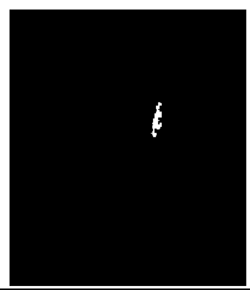	Thrombi
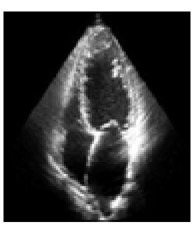 Input Image-3	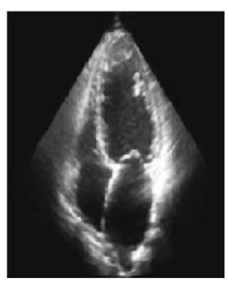		Tumor
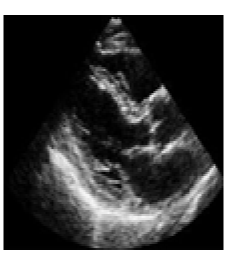 Input Image-4			Tumor

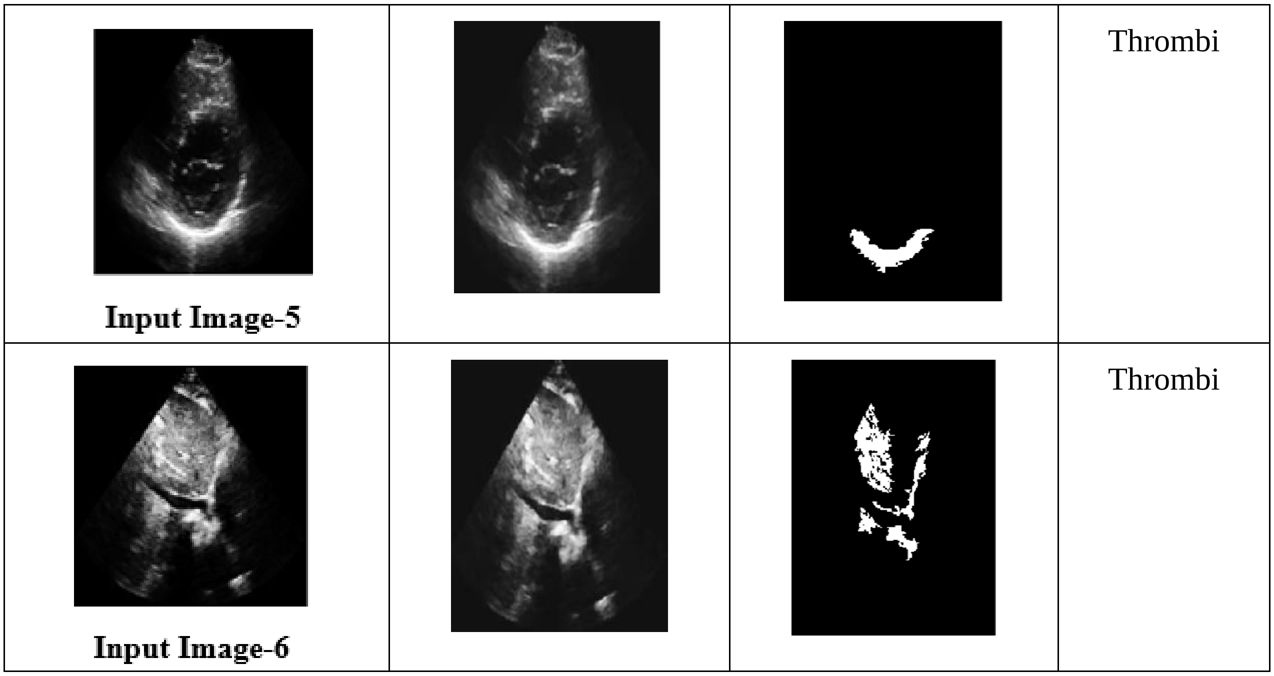

Figure 4. Preprocessing and Segmentation results of Different Intra-Cardiac masses

The simulation result of the preprocessing and segmentation of different samples is shown in Figure 4. The performance analysis of Preprocessing with different filter is listed in Table 1. From the Table 1, the classification results are found as input images 1,2,5,6 are thrombi and images 3, 4 are tumor.

Table 1 depicted the proposed AVMF approach attains the low value of MSE is 8.102 and better value of PSNR is 42.015 dB over the conventional Gaussian and Mean Filter. The proposed MAE value is 0.007687 and SSIM value is 0.671. In this work Mean Squared Error (MSE), Peak Signal to Noise Ratio (PSNR), Mean Absolute Error (MAE) and Structural similarity Index metrics (SSIM) are used to validate preprocessing performance. This comparison clearly shows the proposed AVMF gives good results because some of the edges and image details are not very clear in existing methods, especially at transitions between image regions. But the proposed method perfectly enhances the edges.

Table 1. Performance Evaluation of Filtering Response

Different Parameters	Different Filters	Image 1	Image 2	Image 3	Image 4	Image 5	Image 6	Avg. value of 108 Images
MSE (dB)	Gaussian	14.394	13.869	15.698	14.782	13.698	15.695	16.78
	Mean	11.553	11.569	13.692	12.089	10.859	13.126	13.256
	AVM	7.753	8.693	9.630	8.963	7.631	8.425	8.102
MAE (dB)	Gaussian	0.034830	0.035789	0.03489	0.03671	0.03283	0.03297	0.034731
	Mean	0.025795	0.02498	0.02681	0.02691	0.02479	0.02579	0.028421
	AVM	0.008532	0.00798	0.00793	0.00792	0.00753	0.00947	0.007687
PSNR(dB)	Gaussian	30.895	32.569	33.698	31.896	32.584	33.698	32.56
	Mean	33.886	34.875	37.960	34.871	35.612	36.742	35.98
	AVM	41.646	40.894	41.467	40.569	41.871	41.968	42.015
SSIM	Gaussian	0.571	0.565	0.562	0.568	0.561	0.573	0.578
	Mean	0.609	0.607	0.610	0.614	0.604	0.602	0.603
	AVM	0.672	0.680	0.675	0.678	0.677	0.673	0.671

Table 2 discusses the performance evaluation of segmentation using Global Consistency Error and DICE coefficient with different methods. This comparison clearly shows the proposed Linear Iterative Vessel Segmentation method obtain a good segmentation ratio compared with K-means and fuzzy C-means clustering methods because the Linear Iterative Vessel Segmentation algorithm generates superpixels by clustering pixels based on their color similarity and proximity in the image plane.

Table 2. Performance evaluation of Segmentation Ratio.

Different Parameters	**Different Segmentation**	**Image 1**	**Image 2**	**Image 3**	**Image 4**	**Image 5**	**Image 6**	**Avg. value of 108 Images**
Global Consistency Error(dB)	K-means clustering	0.4615	0.4521	0.4896	0.4715	0.4612	0.4487	0.4661
	FCM clustering	0.4361	0.4389	0.4516	0.4579	0.4316	0.4284	0.4437
	LIVS	0.3619	0.3542	0.3498	0.3371	0.3618	0.3701	0.3558
DICE Coefficie	K-means clustering	0.64	0.62	0.68	0.65	0.66	0.67	0.62
	FCM clustering	0.81	0.79	0.84	0.82	0.84	0.83	0.82
	LIVS	0.96	0.98	0.95	0.92	0.97	0.94	0.95

The proposed LIVS has low GCE inconventional K-means clustering and fuzzy C-means (FCM) clustering methods. The average value of Global Consistency Error rate was 0.3558 for LIVS segmentation over existing methods Fuzzy C means clustering is 0.4437 and K means clustering is 0.4661 of total 108 cardiac images. The average value of DICE coefficient value is 0.95

Comparison of Features Subsets

Table 3 features were used to calculate additional classifications, bringing to a total of 11. Subgroup features that are present in all 9 subgroup features were discovered. Mass movement and base length were mentioned in the characterizations of the cardiologist. They were all about features of cardiologists, their traditional features, and their newer texture feature sets.

Table3. Features for Normal, Cardiac Tumor and Cardiac Thrombi Images

Features	**Normal (Mean±SD)**	**Cardiac Tumor (Mean±SD)**	**Cardiac Thrombi (Mean±SD)**
Standard deviation	1.5634± 0.4011	0.0807±1.9196	0.3161±0.0218
Contrast	0.0845±0.0142	0.02845±0.0324	0.0724±0.0672
Correlation	0.7289±0.0126	0.1244±0.2407	0.5620±0.0236
Energy	1.7834±0.0248	0.7833±0.3889	0.9326±0.0278
Entropy	2.2351±0.1737	0.7270±0.9234	0.5231±0.1340
Homogeneity	2.1427±0.0207	0.9323±0.0158	0.9394±0.0054
LBP1	3.2314±0.1361	1.4299±0.4938	1.7744± 0.217
LBP2	3.3325±0.0252	1.5374±0.0340	1.7734±0.894
LBP5	1.7631±0.1972	0.4923±0.6536	0.6489±0.3908
LBP9	1.9480±0.0324	0.4697±0.0504	0.5550±0.1113
Mean intensity	3.1248±0.02719	0.9402±0.0218	1.26143±0.0267

*SD – Standard Deviation

The simulation result for the Area Under – Receiver operating characteristics Curve (AU-ROC) is shown in Figure 5. This conclusion is supported by these results, which demonstrate that the AU-ROC response is equal to one.

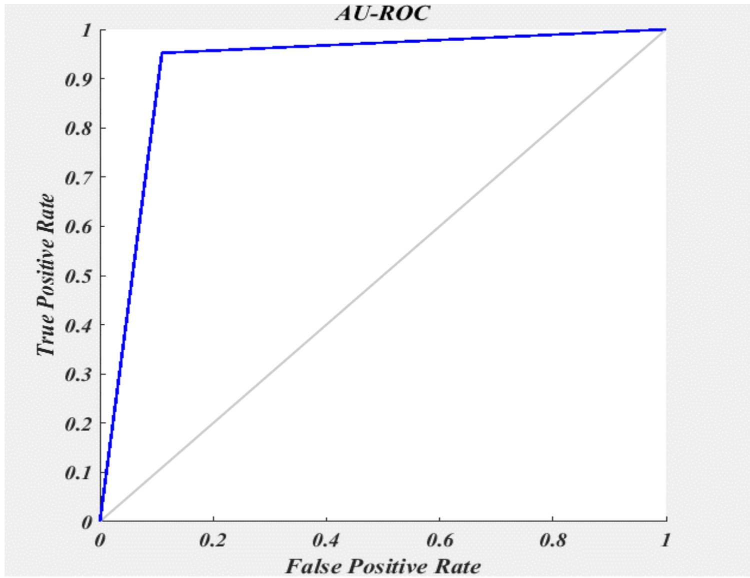

Figure 5. AU-ROC Curve.

Table 4. Overall Performance analysis of classifier based on best feature selection.

Performance Metrics	All 11 features	Only the feature subset of cardiologists	Only the traditional feature subset	Only the new feature texture subset
Accuracy	98.96% (96/108)	98.94% (94/108)	91.76% (75/108)	98.93% (89/108)
Sensitivity	96.17% (54/54)	97.44% (51/54)	85.44% (51/54)	97.03% (47/54)
Specificity	94.33% (42/54)	95.55% (43/54)	81.11% (23/54)	95.11% (41/54)
Positive Prediction	96.91% (56/59)	96.22% (51/53)	85.67% (53/75)	96.11% (48/57)
Negative Prediction	98.56% (40/49)	93.49% (43/55)	87.5% (21/33)	95.41% (41/51)

The results have shown in Table 4 shows the effectiveness of the proposed method when different feature sets are used. Overall classification accuracy is 98.93%. When all 11 features were used as expected, the highest rating was obtained.

Overall Performance:

In this proposed work, 108 real time images collected from Hospital were used for training and testing. Out of this, 80 images were used for training and 28 images used for testing. For 5-fold cross validation, 80 images used as 5 different classes and each class used 20 images as shown in Table 5.A cross-validation was performed using a five-fold analysis. The experiment used 100 epochs and a mini-batch size of 8.The accuracy 98.85% achieved using our proposed RBPNN classifier is better than other state-of-the-arts techniques are SVM-PSO, KCR, Sparse Represent, ANN and SVM in Table 6. The reason for this improvement in classification accuracy is due to the ability of extracting the influential features in decrementing the type of cardiac masses using MS-LBP feature extraction with 5 fold cross validation method and SPSS tool.

Table 5.5-fold; 80% data in training set, 20% in test.

Cardiac Masses Classifier	Iteration 1	Iteration 2	Iteration 3	Iteration 4	Iteration 5
SVM	89.25	91.48	90.91	91.36	90.57
ANN	91.38	91.28	92.49	91.8	91.84
Sparse Representation	92.89	93.47	93.56	91.76	92.65
KCR	92.16	94.73	93.78	93.35	93.49
SVM-PSO	94.65	96.43	94.12	94.13	94.89
RBPNN	**98.46**	**97.67**	**98.89**	**98.38**	**98.65**

Table 6. Comparison of the overall performance evaluation with different classifiers.

Cardiac Masses Classifier		Accuracy (%)	Sensitivity (%)	Specificity (%)	PPV (%)	NPV (%)
SVM	**Real Time Data Set (108 Cardiac Masses Images)**	90.33	95.28	87.78	88.14	97.74
ANN		91.98	92.78	82.39	92.1	96.93
Sparse Representation		92.48	94.47	83.65	94.74	96.23
KCR		93.92	94.89	87.23	94.98	95.973
SVM-PSO		94.55	96.79	89.82	96.29	95.34
RBPNN		**98.85**	**97.38**	**98.31**	**98.6**	**94.5**

Run Time Analysis:

The running time of the proposed method was calculated for each processing and it took about 412.782 seconds to analyze and identify the cardiac masses, where it took 290.45 seconds to eliminate the noise and to segment the masses, took 110.75 seconds.

State of art techniques

Table7. State of art techniques classification of the conventional classifier

Cardiac Masses Classifier	Cardiac masse Image Dataset	Accuracy	Sensitivity	Specificity
SVM [15]	Echocardiogram	92.79	89.89	90.91
ANN [13]	Echocardiogram	84.65	87.78	86.94
Sparse Representation [5]	Echocardiogram	92.48	90.33	91.98
SVM-PSO [19]	CT	96.23	97.74	96.93
KCR [17]	MRI	94.74	88.14	92.1
RBPNN	**Echocardiogram**	**98.85**	**97.38**	**98.31**

The accuracy 98.85% achieved using our proposed RBPNN classifier is better than other state-of-the-arts techniques are SVM-PSO, KCR, Sparse Represent, ANN and SVM in Table 8. The reason for this improvement in classification accuracy is due to the ability of extracting the influential features in decrementing the type of cardiac masses using MS-LBP feature extraction. The proposed adaptive vector median filters suppressed the noise very effectively while maintaining fine details and very well, and filter performance over conventional filters. The Linear Iterative Vessel Segmentation algorithm clusters pixels based on color similarity and proximity in the image plane to generate superpixels. The MSLBP description shows the local texture capabilities of an image by comparing each pixel to an adjacent pixel. The method provided contains the complete structural information extracted by the Local Binary Patterns and uses the size information to extract additional information to get additional discriminative power.

CONCLUSION

In this work, a robust back propagation neural network (RBPNN) scheme is proposed to detect and classify the intra-cardiac masses from echocardiogram images. Initially, the noise is diminished from echocardiogram images utilizing the adaptive vector median filter. The masses were automatically segmented dependent on linear iterative vessel segmentation strategy followed by texture features extracted utilizing the multiscale local binary pattern method. These features were used to separate the intracardiac mass from the echocardiogram images using an RBPNN with conventional Sparse Representation, SVM-PSO, SVM, ANN and KCR methods. The Accuracy, sensitivity, and specificity suggested RBPNN system are 98.85%, 97.38%, and 98.31%. More prominent productivity and basic execution make the RBPNN approach helpful for cardiologists to make anticipation before medical surgery.

Conflict of interest: The authors declare that they have no conflict of interest.

Acknowledgements: The authors are grateful to Department of Echocardiography, Vinayaka Mission's Kirupananda Variyar Medical College & Hospital, Salem, Tamil Nadu for providing the Echocardiogram database of cardiac masses images.

REFERENCES

1. Pedrosa J, Queiros S, Bernard O, Engvall J, Edvardsen T, Nagel E, et al.Fast and Fully Automatic Left Ventricular Segmentation and Tracking in Echocardiography Using Shape-Based B-Spline Explicit Active Surfaces. IEEE Trans Med Imaging. 2017 Nov;36(11):2287-96. doi: 10.1109/TMI.2017.2734959. Epub 2017 Aug 2. PMID: 28783626.
2. Peressutti D, Gomez A, Penney GP, King AP. Registration of Multiview Echocardiography Sequences Using a Subspace Error Metric. IEEE Trans Biomed Eng. 2017 Feb;64(2):352-61. doi: 10.1109/TBME.2016.2550487. PMID: 28113189.
3. Wildes D, Lee W, Haider B, Cogan S, Sundaresan K, Mills DM, et al. 4-D ICE: A 2-D Array Transducer With Integrated ASIC in a 10-Fr Catheter for Real-Time 3-D Intracardiac Echocardiography. IEEE Trans UltrasonFerroelectr Freq Control. 2016 Dec;63(12):2159-73. doi: 10.1109/TUFFC.2016.2615602. Epub 2016 Oct 12. PMID: 27740477.
4. Yu L, Zhou Z, He B. Temporal Sparse Promoting Three Dimensional Imaging of Cardiac Activation. IEEE Trans Med Imaging. 2015 Nov;34(11):2309-19. doi: 10.1109/TMI.2015.2429134. Epub 2015 May 4. PMID: 25955987; PMCID: PMC4652642.
5. Guo Y, Wang Y, Kong D, Shu X. Automatic classification of intracardiac tumor and thrombi in echocardiography based on sparse representation. IEEE J Biomed Health Inform. 2015 Mar;19(2):601-11. doi: 10.1109/JBHI.2014.2313132. Epub 2014 Mar 21. PMID: 24691169.
6. Hruska CB, O'Connor MK. Nuclear imaging of the breast: translating achievements in instrumentation into clinical use. Med Phys. 2013 May;40(5):050901. doi: 10.1118/1.4802733. PMID: 23635248; PMCID: PMC3656956.
7. Xie Y, Zhang W, Li C, Lin S, Qu Y, Zhang Y. Discriminative object tracking via sparse representation and online dictionary learning. IEEE transactions on cybernetics. 2013 May 31;44(4):539-53.
8. Khoury DS, Liyun Rao, Panescu D. Contrast echocardiography for cardiac radio-frequency ablation. IEEE Pulse. 2011 Sep-Oct;2(5):56-64. doi: 10.1109/MPUL.2011.942606. PMID: 25372970.
9. Abramyuk A, Wolf G, Hietschold V, Haberland U, Van den Hoff J, Abolmaali N. Comment on "Developing DCE-CT to quantify intra-tumor heterogeneity in breast tumors with differing angiogenic phenotype". IEEE Trans Med Imaging. 2010 Apr;29(4):1088-9; author reply 1089-92. doi: 10.1109/TMI.2009.2031780. PMID: 20659827.

10. Oksuz I, Mukhopadhyay A, Dharmakumar R, Tsaftaris SA. Unsupervised Myocardial Segmentation for Cardiac BOLD. IEEE Trans Med Imaging. 2017 Nov;36(11):2228-2238. doi: 10.1109/TMI.2017.2726112. Epub 2017 Jul 12. PMID: 28708550; PMCID: PMC5726889.
11. Cao M, Liang Y, Shen C, Miller KD, Stantz KM. Developing DCE-CT to quantify intra-tumor heterogeneity in breast tumors with differing angiogenic phenotype. IEEE Trans Med Imaging. 2009 Jun;28(6):861-71. doi: 10.1109/TMI.2008.2012035. Epub 2009 Jan 13. PMID: 19150783.
12. Martin-Isla C, Campello VM, Izquierdo C, Raisi-Estabragh Z, Baeßler B, Petersen SE, et al. Image-Based Cardiac Diagnosis With Machine Learning: A Review. Front Cardiovasc Med. 2020 Jan 24;7:1. doi: 10.3389/fcvm.2020.00001. PMID: 32039241; PMCID: PMC6992607.
13. Strzelecki M, Materka A, Drozdz J, Krzeminska-Pakula M, Kasprzak JD. Classification and segmentation of intracardiac masses in cardiac tumor echocardiograms. Comput Med Imaging Graph. 2006 Mar;30(2):95-107. doi: 10.1016/j.compmedimag.2005.11.004. Epub 2006 Feb 14. PMID: 16476535.
14. Meng J, Zhao H, Liu Y, Chen D, Hacker M, Wei Y, et al. Assessment of cardiac tumors by ^{18}F-FDG PET/CT imaging: Histological correlation and clinical outcomes. J NuclCardiol. 2021 Oct;28(5):2233-2243. doi: 10.1007/s12350-019-02022-1. Epub 2020 Jan 13. PMID: 31933156.
15. Gerber TC, Foley DA, Zheng Y, Behrenbeck T, Tajik AJ, Seward JB. Differentiation of intracardiac tumors and thrombi by echocardiographic tissue characterization: comparison of an artificial neural network and human observers. Echocardiography. 2000 Feb;17(2):115-26. doi: 10.1111/j.1540-8175.2000.tb01112.x. Erratum in: Echocardiography 2000 May;17(4):iv. PMID: 10978969.
16. Burazor I, Aviel-Ronen S, Imazio M, Goitein O, Perelman M, Shelestovich N, et al. Metastatic cardiac tumors: from clinical presentation through diagnosis to treatment. BMC Cancer. 2018 Feb 20;18(1):202. doi: 10.1186/s12885-018-4070-x. PMID: 29463229; PMCID: PMC5819646.
17. Guo Y, Wang Y, Kong D, Shu X. Automatic Classification of Intracardiac Tumor and Thrombi in Echocardiography Based on Sparse Representation.IEEE Journal of Biomedical and Health Informatics*, 2015;19*, 601-11.
18. Amano J, Nakayama J, Yoshimura Y, Ikeda U. Erratum to: Clinical classification of cardiovascular tumors and tumor-like lesions, and its incidences. Gen Thorac Cardiovasc Surg. 2013;61(8):448. doi: 10.1007/s11748-013-0244-2. Epub 2013 May 21. Erratum for: doi: 10.1007/s11748-013-0214-8. PMCID: PMC4079610.
19. Li X, Chen Y, Liu J, Xu L, Li Y, Liu D, et al. Cardiac magnetic resonance imaging of primary cardiac tumors. Quant Imaging Med Surg. 2020 Jan;10(1):294-313. doi: 10.21037/qims.2019.11.13. PMID: 31956550; PMCID: PMC6960432.
20. Stendahl JC, Parajuli N, Lu A, Boutagy NE, Guerrera N, Alkhalil I, et al.Regional myocardial strain analysis via 2D speckle tracking echocardiography: validation with sonomicrometry and correlation with regional blood flow in the presence of graded coronary stenoses and dobutamine stress. Cardiovasc Ultrasound. 2020 Jan 15;18(1):2. doi: 10.1186/s12947-019-0183-x. PMID: 31941514; PMCID: PMC6964036.